Review of Scientific Instruments

A new B-dot probe circuit for magnetic diagnostics of radio frequency discharges

Cite as: Rev. Sci. Instrum. **89**, 105104 (2018); https://doi.org/10.1063/1.5041814
Submitted: 26 May 2018 . Accepted: 18 September 2018 . Published Online: 04 October 2018

Kai Zhao, Yong-Xin Liu, De-Qi Wen, Demetre J. Economou, and You-Nian Wang

A new B-dot probe circuit for magnetic diagnostics of radio frequency discharges

Kai Zhao,[1,2] Yong-Xin Liu,[1] De-Qi Wen,[1] Demetre J. Economou,[2] and You-Nian Wang[1,a)]
[1]*Key Laboratory of Materials Modification by Laser, Ion, and Electron Beams (Ministry of Education), School of Physics, Dalian University of Technology, Dalian 116024, China*
[2]*Plasma Processing Laboratory, Department of Chemical and Biomolecular Engineering, University of Houston, Houston, Texas 77204-4004, USA*

(Received 26 May 2018; accepted 18 September 2018; published online 4 October 2018)

Accurate magnetic measurements in radio frequency capacitively coupled plasmas (CCP) are challenging due to the presence of inherently strong electric fields and relatively weak magnetic fields. In this work, a new B-dot probe circuit is presented, comprising two variable capacitors in a tunable series resonance circuit, with a center-tapped, step-up transformer. The output characteristics of the probe are predicted using two distinct equivalent circuit models, one for the differential mode and the other for the common mode. A Helmholtz coil and a Faraday cup are used for experimental validation of the predicted probe output. By tuning the two variable capacitors in the circuit, the magnetic probe can achieve improved signal-to-noise ratio by amplifying the inductive signal, while suppressing capacitive coupling interference. Using the newly designed probe, magnetic measurements in typical CCP are presented. *Published by AIP Publishing.* https://doi.org/10.1063/1.5041814

I. INTRODUCTION

The B-dot probe is a workhorse for measuring the magnetic induction in a variety of plasma devices.[1–7] Particularly in inductively coupled plasmas (ICP), magnetic field measurements allow visualization of the spatial distribution of radio frequency (rf) current density, electric field as well as power deposition in the reactor, providing insights into important physics, such as the anomalous skin effect.[8,9] On the other hand, accurate measurements of the magnetic field in capacitively coupled plasmas (CCP) are challenging because of the inherently weak magnetic field, and the so-called capacitive pickup,[10] which stems from the capacitive coupling between the oscillating plasma potential and the probe coil, causing serious interference.

In order to improve the signal-to-noise ratio of the B-dot probe, one has to increase the inductive signal output (i.e., improve the magnetic sensitivity) and/or suppress the capacitive signal output (i.e., enhance the capacitive pickup rejection). Traditionally, one utilizes a step-up transformer to increase the B-dot output.[11] An alternative method is to use an amplifier.[12] On the other hand, a common method to suppress the capacitive signal output is to reduce the potential difference between the plasma and the probe coil, for example, by using a coaxial cable in series with the probe coil. By comparing several of the most commonly used magnetic probe designs, Franck *et al.*[13] reported that the center-tapped transformer (CTT) exhibited optimal performance for rejecting capacitive pickup. More recently, Sun *et al.*[14] proposed a tunable magnetic probe with a CTT to improve the signal-to-noise ratio. It was difficult, however, to eliminate the electrical asymmetry caused by the rotary variable capacitor used.

In this work, we propose a new tunable series resonance circuit for a B-dot probe for magnetic diagnostics of rf discharges. The circuit is designed geometrically symmetric with respect to the center tap; moreover, we introduce two symmetrical variable capacitors to eliminate the electrical asymmetry. As will be shown below, the electrical symmetry can be ensured by tuning these two variable capacitors, eventually achieving a minimum capacitive interference signal. Meanwhile, the inductive signal can be highly amplified.

This paper is organized as follows. The details of the B-dot probe design are described in Sec. II. In Sec. III, by employing two distinct equivalent circuit models and well-defined experiments, we present the output characteristics of the magnetic probe. Magnetic induction measurements in a typical CCP reactor are shown in Sec. IV before concluding.

II. PROBE DESIGN

Miniaturization, high magnetic sensitivity, and high capacitive pickup rejection are the three most desirable characteristics of a magnetic probe. To achieve these characteristics, one must pay particular attention to the following: (i) probe coil design, (ii) probe shaft and enclosure, (iii) electrostatic shielding, and (iv) signal processing circuit.

Figure 1(a) illustrates a schematic of the magnetic probe. The probe head is a two-turn circular coil with a diameter of $d_0 = 3$ mm, made of 0.51 mm-diameter enameled copper wire. The two ends of the coil are twisted in pairs and welded to the inner conductors of two 60 cm-length semirigid coaxial cables (SFT50-1). To reduce the influence of plasma potential oscillations on the probe shaft, the coaxial cables are wrapped with a grounded aluminum foil and then inserted into a supporting quartz tube. The other ends of the two cables are terminated by the subminiature version A (SMA) connectors, which can

a)Electronic mail: ynwang@dlut.edu.cn

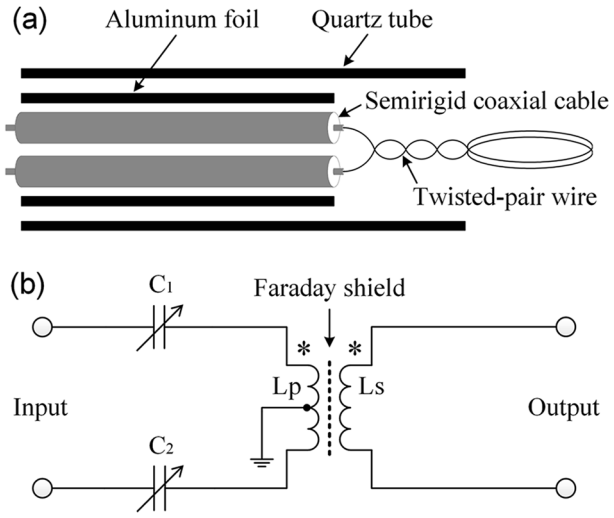

FIG. 1. Schematics of the magnetic probe (a) and the signal processing circuit (b). Variable capacitors C_1 and C_2 are tuned to obtain electrical symmetry.

be connected to the input ports of the signal processing circuit [Fig. 1(b)].

The signal processing circuit is primarily composed of a tunable series resonance circuit coupled with a center-tapped, step-up transformer. A sketch of the center-tapped, step-up transformer is illustrated in Fig. 2. It consists of a 2-turn primary winding and a 3-turn secondary winding. Both windings are made of enamelled copper wire 0.8 mm in diameter, wound on a circular spool frame with an outer diameter of 70 mm. A center tap connects the geometric center of the primary winding to ground. Electrical measurements were carried out using an RLC meter (Tonghui TH2822C), with standard "short" and "open" corrections, at room temperature. The inductances of the primary and secondary windings were 1.78 and 2.75 μH, respectively. The primary winding features two variable capacitors, forming a series resonant circuit. These capacitors are placed in geometrically symmetric positions with respect to the center tap, in order to promote circuit symmetry. The secondary winding is connected to the output port of the circuit. A Faraday shield, fabricated by a single-sided printed circuit board (PCB) with a comb-like pattern, is placed between the primary and secondary windings to suppress capacitive coupling.

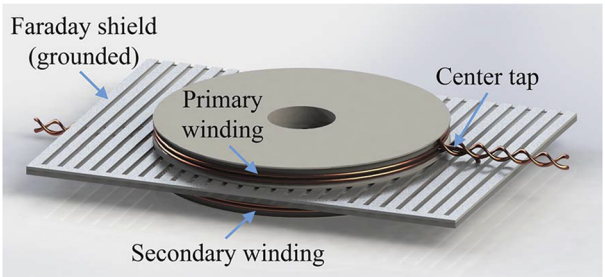

FIG. 2. Sketch of the center-tapped, step-up transformer. The turns ratio of the primary-to-secondary windings of the transformer is 1:1:3. A Faraday shield is placed between the primary and secondary windings to suppress capacitive coupling. No ferrite core is employed.

III. PROBE OUTPUT CHARACTERISTICS

To gain insight into the output characteristics of the B-dot probe, two distinct equivalent circuit models are used. The output signal of the probe can be regarded as a superposition of two components: (i) the inductive component caused by the time derivative of the magnetic flux [the differential mode (DM) signal] and (ii) the capacitive component resulting from capacitive coupling between the plasma and the probe coil [the common mode (CM) signal]. In this section, we will briefly describe these two modes followed by modeling and experimental results.

A. Differential mode (DM) signal output

A schematic of the equivalent circuit for the DM signal is shown in Fig. 3(a). The induced voltage in the probe coil can be considered an ideal voltage source $U_{id}(t) = -j\omega naB_0 e^{j\omega t}$, where ω and B_0 represent the angular frequency and the amplitude of the time-varying magnetic field, respectively. Furthermore, n and a denote the number of turns and the cross-sectional area of the probe coil, respectively. The primary circuit consists of two coaxial cables (Z_1 and Z_2), two variable capacitors (C_1 and C_2), and the inductance (L_p) and resistance (R_p) of the primary winding. The secondary circuit includes a coaxial cable (Z_3), and the inductance (L_s) and resistance (R_s) of the secondary winding. The load is the input impedance Z_{in} of the oscilloscope. The coaxial cables are assumed to be lossless so that the propagation constant of the transmission line is purely imaginary ($\gamma = j\beta$, where β is the phase-shift coefficient). Furthermore, in the presence of the Faraday shield, the capacitive coupling between the primary and secondary windings of the transformer is neglected in this circuit model.

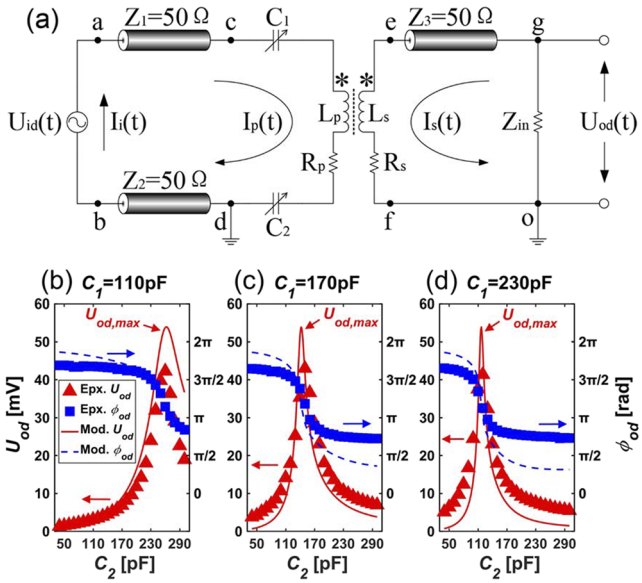

FIG. 3. (a) Schematic diagram of the equivalent circuit for the differential mode signal, with all outer conductors of the coaxial cables assumed to be grounded; model predictions (lines) and experimental data (points) of the DM signal output (U_{od} and ϕ_{od}) as a function of C_2, for different values of C_1: (b) C_1 = 110 pF, (c) C_1 = 170 pF, and (d) C_1 = 230 pF.

The DM signal output is investigated experimentally using a Helmholtz coil, for producing a well-defined magnetic field. The Helmholtz coil is constructed with a pair of single-turn loops with a radius R_0 = 35 mm, separated by 35 mm. A 13.56 MHz sinusoidal voltage (0–20 V), produced by a function generator (Tektronix AFG3252C), is applied to the Helmholtz coil. The probe coil is positioned at the center of the Helmholtz coil to detect the magnetic induction.

The output signal of the B-dot probe is recorded by using an oscilloscope (LeCroy, Waverunner 104Xi, 1 GHz analog bandwidth, 10 Gs/s). Simultaneously, the current I_{coil} in the Helmholtz coil is measured by using a current monitor (Pearson 6585, 250 MHz bandwidth), through which the magnetic field amplitude B_0 at the center of the Helmholtz coil can be calculated by $B_0 = (4/5)^{3/2}\mu_0 N I_{coil}/R_0$. Here, $\mu_0 = 4\pi \times 10^{-7}$ T m/A is the permeability in free space, and N represents the number of turns of the Helmholtz coil. The coil current is fixed at I_{coil} = 128 mA for all conditions. Based on the above, B_0 and the induced voltage amplitude in the probe coil, U_{id}, are estimated to be 3.29 μT and 3.96 mV, respectively. The magnetic sensitivity, determined by U_{id}/B_0, is about 1.2 mV/μT, quite a small value.

Figures 3(b)–3(d) show model predictions (lines) and experimental data (points) of the variation of the DM output voltage amplitude U_{od} and the relative phase ϕ_{od} [with respect to the current $I_{coil}(t)$ in the Helmholtz coil] as a function of C_2, for different values of C_1. Reasonably good agreement between modeling and experiment, for both U_{od} and ϕ_{od}, is observed. For every value of C_1 tested, U_{od} goes through a maximum ($U_{od,\max}$) as a function of C_2, at which ϕ_{od} exhibits an abrupt change. In quantitative terms, $U_{od,\max}$ can reach 42 mV by tuning C_2 for given C_1, which is more than one order of magnitude greater than U_{id} (~3.96 mV); correspondingly, the magnetic sensitivity is improved from 1.2 to 12.8 mV/μT. These results are indicative of a typical series resonance characteristic. By increasing C_2, the circuit transitions from capacitive reactance to inductive reactance. Resonance occurs at the so-called "resonance point" where the inductive reactance is equal to the capacitive reactance, resulting in minimum impedance and, thus, maximum current. Apart from the series resonance circuit, the step-up transformer also plays an important role in amplifying U_{od}.

B. Common mode (CM) signal output

A schematic diagram of the equivalent circuit for the CM signal is illustrated in Fig. 4. Compared to the DM case, only the primary circuit is changed. In this scenario, the fluctuating potential difference between plasma and probe coil can be represented by an ideal voltage source $U_{ic}(t)$. The capacitive current flows through two branches, i.e., a-c and b-d, and then goes via the center tap to ground. In the a-c branch, the coaxial cable (Z_1), variable capacitor (C_1), and half of the inductance ($L_p/2$) and half of the resistance ($R_p/2$) in the primary winding are in series. A symmetric, series connection involves Z_2, C_2, $L_p/2$, and $R_p/2$ in the b-d branch.

Experimentally, the CM signal output was investigated by using a Faraday cup, which is employed to produce a

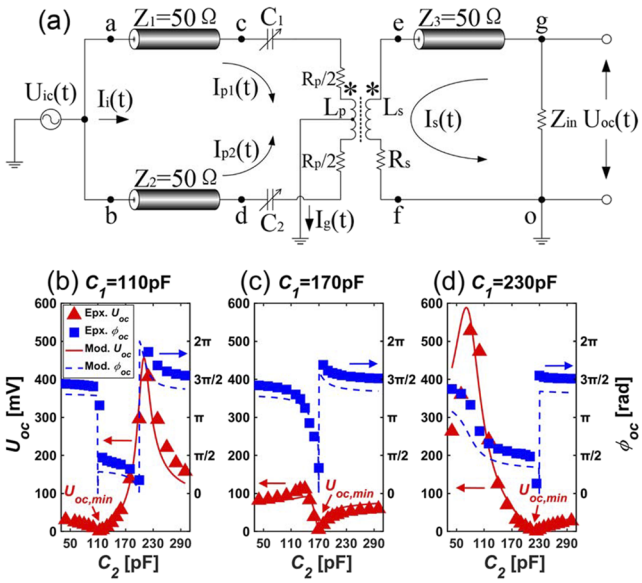

FIG. 4. (a) Schematic diagram of the equivalent circuit for the common mode signal, with all outer conductors of the coaxial cables assumed to be grounded; model predictions (lines) and experimental data (points) of the CM signal output (U_{oc} and ϕ_{oc}) as a function of C_2, for different values of C_1: (b) C_1 = 110 pF, (c) C_1 = 170 pF, and (d) C_1 = 230 pF.

homogeneous electric field. The Faraday cup is 160 mm in length and 40 mm in inner diameter, and it is mechanically fastened to a grounded box. A 13.56 MHz rf voltage generated by using a power amplifier is applied to the Faraday cup. The probe coil is inserted into the center of the Faraday cup to detect the capacitive signal. The voltage amplitude U_{cup} on the Faraday cup is measured by using a high-voltage probe (Tektronix P6015A). Here, U_{cup} is kept at 100 V for all conditions. Accordingly, assuming that the probe coil has a 1.5 pF coupling to the Faraday cup/plasma, the amplitude of $U_{ic}(t)$ is estimated to be about 102 mV.

Figures 4(b)–4(d) display the dependence of the CM output [voltage amplitude U_{oc} and phase ϕ_{oc} with respect to the voltage $U_{cup}(t)$] on C_2, for different values of C_1. Again a reasonably good agreement between model predictions and experimental data is observed. The variation of U_{oc} with C_2 is more complicated compared to U_{od} [see Figs. 3(b)–3(d)]. At C_1 = 110 pF, U_{oc} is observed to first slowly decrease with C_2 and then to rise sharply, going through a maximum. However, at larger C_1 (i.e., 170 pF and 230 pF), U_{oc} first increases with C_2, reaches a maximum, and then goes through a minimum, a behavior not seen at C_1 = 110 pF.

From Fig. 4, one can draw the following conclusions. (i) For given C_1, two extreme values (a maximum $U_{oc,\max}$ and a minimum $U_{oc,\min}$) occur in the curve of U_{oc} vs. C_2. Around each extreme value, an abrupt change in ϕ_{oc} is clearly observed. (ii) In the vicinity of $U_{oc,\max}$, the abrupt change in ϕ_{oc} is supposed to be caused by electrical resonance; i.e., by increasing C_2, an impedance transition occurs, leading to an abrupt change in the current phase, which is very similar to the cases in Fig. 3. (iii) In the vicinity of $U_{oc,\min}$, the abrupt change in ϕ_{oc} is related to the change in the net current direction in the primary winding.

Results presented thus far demonstrate that for given C_1, $U_{oc,\min}$ can reach a minimum value (~0) by tuning C_2. Under the condition $U_{oc,\min} = 0$, the branch currents I_{p1} (in a-c branch) and I_{p2} (in b-d branch) are identical both in amplitude and in phase so that they cancel out, leading to suppression of capacitive pickup. In short, the main role of the two variable capacitors is to balance the capacitive currents flowing through the two branches to the ground, when operated in the CM mode. In addition, as important elements in the series resonant circuit, these capacitors also play a role in amplifying the inductive signal, when operated in the DM mode.

In order to achieve the highest signal-to-noise ratio, $U_{od,\max}$ in the DM mode and $U_{oc,\min}$ in the CM case must occur at the same value of C_2. This can be achieved, according to the results shown in Figs. 3 and 4. In Figs. 3(b)–3(d), with increasing C_1, the corresponding C_2 for obtaining $U_{od,\max}$ gradually decreases. By contrast, in Figs. 4(b)–4(d), with increasing C_1, the corresponding C_2 for obtaining $U_{oc,\min}$ gradually increases. Thus, by increasing C_1, there is a certain value of C_2 at which $U_{od,\max}$ and $U_{oc,\min}$ occur simultaneously; this is the optimal operating point. Figure 5 illustrates modeling and experimental data for obtaining the optimal operating point, which occurs at $C_1 = C_2 = 155$ pF.

It is worth mentioning that, in addition to the two variable capacitors (C_1 and C_2), the output characteristics of the B-dot probe can be significantly affected by the length of the coaxial cables (Z_1, Z_2, and Z_3) and the turns of the transformer windings, which determine the inductance of the circuit and thus the resulting resonant behavior. In addition, changing the coaxial cables and the transformer windings can shift the optimal operating point. Therefore, the performance to suppress capacitive pickup can also be affected. On the other hand, the amplification of the B-dot probe depends not only on the coupling coefficient of the transformer but also on the quality factor of the LC resonance circuit. Hence, proper sizes of the coaxial cables and transformer windings are crucial for achieving a satisfactory/stable performance of the device. Furthermore, it should be noted that the optimal operating point strongly depends on the working frequency and is also sensitive to changes in temperature.

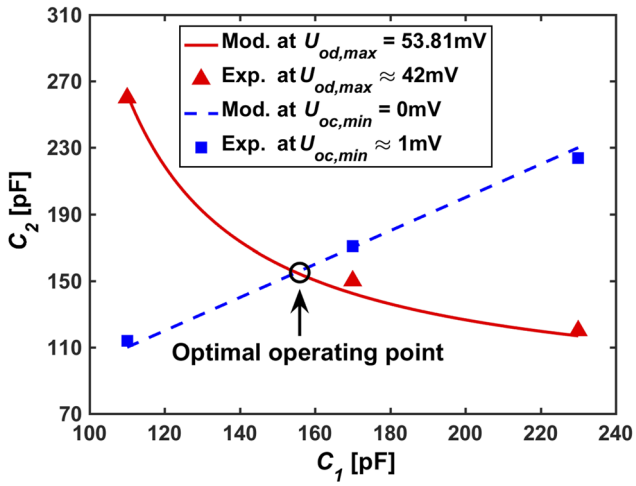

FIG. 5. Model predictions (lines) and experimental data (points) of C_2 (at different values of C_1) for obtaining $U_{od,\max}$ in the DM case and $U_{oc,\min}$ in the CM case. The intersection between the solid and dashed lines defines the optimal operating point.

IV. MAGNETIC MEASUREMENTS IN A CCP REACTOR

The B-dot probe was tested in a typical CCP reactor[15,16] to further evaluate its performance. An argon plasma was sustained at 3 Pa, by a 13.56 MHz power supply with a fixed output power of 100 W. The diameter of the parallel plate electrodes was 21 cm. The measurement point was located at $r = 10$ cm close to the electrode edge. In order to clarify the crucial roles of the probe circuit, a comparative experiment was performed under three different circuit conditions: (i) without any tuning capacitor, (ii) with a single tuning capacitor, and (iii) with both tuning capacitors. For each situation, we measured the raw signals from the B-dot probe for three different probe orientations; i.e., the plane of the probe coil is perpendicular to the electrodes ($\phi = \pm\pi/2$ to measure the azimuthal component of the magnetic induction B_φ) and parallel to the electrodes ($\phi = 0$ to measure the axial component of the magnetic induction B_z). Measurement results are presented in Fig. 6 and discussed below.

Case I: without any tuning capacitor. In this case, the capacitors C_1 and C_2 illustrated in Figs. 3(a) and 4(a) were removed and replaced by a connecting wire. Without the

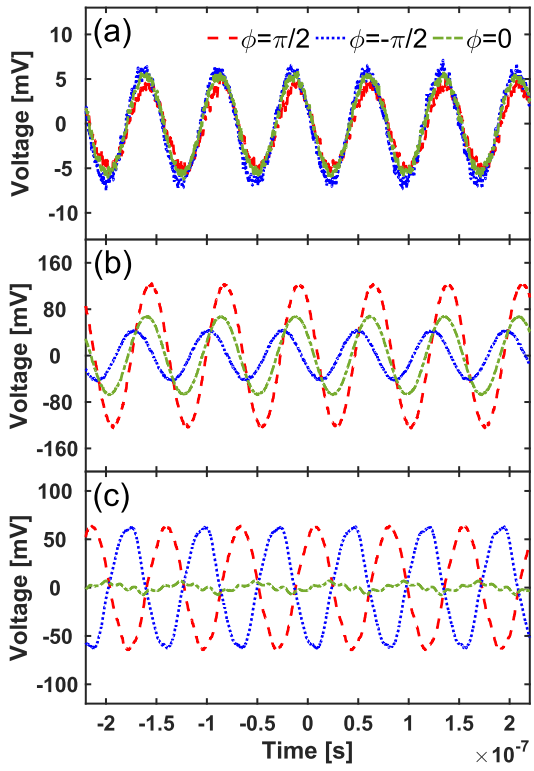

FIG. 6. Comparisons of the raw signals from the B-dot probe output under three different circuit conditions: (a) without any tuning capacitor, (b) with a single tuning capacitor, and (c) with both tuning capacitors. Measurements were performed in a CCP reactor for three probe orientations ($\phi = 0, \pm\pi/2$).

tuning capacitors, the output signals [Fig. 6(a)] are observed to be quite weak as compared to those in the other two cases [Figs. 6(b) and 6(c)]. This could be mainly attributed to a relatively large inductive reactance ($j\omega L_p \sim 152\ \Omega$) of the primary winding in the transformer, which leads to a quite small current/voltage in the primary circuit and, hence, a small induced voltage in the secondary circuit. On the basis of the equivalent circuit of the DM signal, taking an approximate magnetic field intensity ($B_\varphi \sim 4.5\ \mu$T) into account, we estimate that the amplitude of the DM signal is less than 1 mV, quite a small value. This estimation is in accordance with our measurement results. In Fig. 6(a), the signals for all orientations exhibit similar values both in amplitudes and in phases, indicating that the signals detected are mainly caused by the CM interference, whereas the contribution from the DM component is fairly small. These CM signals could be due to the slight asymmetries in the center-tapped, step-up transformer or even the B-dot probe itself.

Case II: with a single tuning capacitor. In this case, only capacitor C_1 was removed and replaced by a connecting wire. Before our experiments, the B-dot probe was tested and calibrated using the Helmholtz coil. By tuning C_2, we operated the probe circuit at the resonance frequency of 13.56 MHz, i.e., a same maximum DM signal as *case III* was achieved. Even so, one can clearly identify from Fig. 6(b) that the amplitude of the output signal in the orientation $\phi = 0$ is sufficiently large compared to the signals in the orientations $\phi = \pm\pi/2$, suggesting that the CM interference is still considerable. Due to the contamination of the DM signal by the CM interference, the signal waveforms in the orientations $\phi = \pm\pi/2$ become highly asymmetric. In practice, when operated at the resonance point, both DM and CM signals can be greatly amplified. Due to the absence of C_1, the circuit asymmetry of the two branches in a-c and b-d, as shown in Fig. 4(a), generates two extremely unbalanced capacitive currents flowing through the two branches to the ground and, thus, a large net current occurs in the primary winding of the transformer, significantly contributing to the output signal.

Case III: with both tuning capacitors. In order to make the probe circuit symmetric, both capacitors were employed in this case. As mentioned before, by tuning capacitors C_1 and C_2, we operated the B-dot probe at the optimal operating point; namely, using the Helmholtz coil and the Faraday cup, $U_{od,\max}$ in the DM mode and $U_{oc,\min}$ in the CM case can be achieved simultaneously. Observed from Fig. 6(c), one can find that the signals in the orientations $\phi = \pi/2$ and $\phi = -\pi/2$ are almost equal in amplitude but out of phase with each other. This coincides with the fact that reversing the external magnetic field will result in reversal of the polarity of the induced voltage in the probe coil, but the amplitude will remain unchanged. In addition, the amplitude of the output signal in the orientation $\phi = 0$ is observed to be negligible compared to the signals in the orientations $\phi = \pm\pi/2$ in accordance with the fact that the axial magnetic field component B_z should be zero in a CCP reactor. The results presented thus demonstrated that with the two-tuning-capacitor circuit the B-dot probe can achieve an improved signal-to-noise ratio by amplifying the inductive signal, while suppressing capacitive coupling interference.

V. CONCLUSIONS

In summary, a new B-dot probe circuit was developed for magnetic diagnostics of radio frequency (rf) discharges. To improve the magnetic sensitivity and enhance the capacitive pickup rejection, attention was paid to the probe coil design, probe shaft and enclosure, electrostatic shielding, as well as the signal processing circuit. The latter was principally composed of a tunable series resonance circuit featuring two variable capacitors, combined with a center-tapped, step-up transformer. In addition, a Faraday shield was placed between the primary and secondary windings of the transformer to further suppress electrostatic capacitive coupling.

We developed two distinct equivalent circuit models to study the output signal of the B-dot probe, including the differential mode (DM) component caused by the time derivative of the magnetic flux and the common mode (CM) component resulting from capacitive coupling between the oscillating plasma potential and the probe coil. For experimental validation, we used a Helmholtz coil to produce a well-defined magnetic field and a Faraday cup to produce a homogeneous electric field. The output characteristics of the B-dot probe were predicted by the circuit models and validated by the experiments. By tuning the two variable capacitors in the circuit, the DM output voltage U_{od} could be highly amplified (as compared to the original output voltage of the probe coil), while the CM output voltage U_{oc} could be substantially reduced, yielding an improved signal-to-noise ratio. Furthermore, the optimal operating condition for achieving the highest signal-to-noise ratio was determined through modeling.

The B-dot probe was tested in a typical CCP reactor to further evaluate its performance. By performing a comparative experiment under three different circuit conditions, i.e., without any tuning capacitor, with a single tuning capacitor, and with both tuning capacitors, the crucial characteristics of the probe circuit were demonstrated.

ACKNOWLEDGMENTS

This work was supported by the National Natural Science Foundation of China (NSFC) (Grant Nos. 11335004 and 11722541). D.J.E. acknowledges support from the National Science Foundation (No. PHY-1500518) and the Department of Energy, Office of Fusion Energy Science (No. DE-SC0014132). K.Z. acknowledges financial support from the China Scholarship Council. The authors gratefully acknowledge Peng-Cheng Du and Xiang-Yu Wang for experimental assistance.

[1] P. V. Savrukhin and E. A. Shestakov, Rev. Sci. Instrum. **83**, 013505 (2012).
[2] E. J. Strait, Rev. Sci. Instrum. **77**, 023502 (2006).
[3] V. A. Godyak and V. I. Kolobov, Phys. Rev. Lett. **79**, 4589 (1997).
[4] J. Hopwood, C. R. Guarnieri, S. J. Whitehair, and J. J. Cuomo, J. Vac. Sci. Technol., A **11**, 147 (1993).
[5] V. A. Godyak and R. B. Piejak, J. Appl. Phys. **82**, 5944 (1997).
[6] W. Gekelman, A. Collette, and S. Vincena, Phys. Plasmas **14**, 062109 (2007).
[7] E. T. Everson, P. Pribyl, C. G. Constantin, A. Zylstra, D. Schaeffer, N. L. Kugland, and C. Niemann, Rev. Sci. Instrum. **80**, 113505 (2009).

[8]Z. F. Ding, B. Sun, and W. G. Huo, Phys. Plasmas **22**, 063504 (2015).
[9]V. A. Godyak, R. B. Piejak, B. M. Alexandrovich, and V. I. Kolobov, Phys. Rev. Lett. **80**, 3264 (1998).
[10]F. F. Chen, in *Plasma Diagnostic Techniques*, edited by R. H. Huddlestone and S. L. Leonard (Academic, NY, 1965).
[11]D. C. Black and R. M. Mayo, Rev. Sci. Instrum. **67**, 1508 (1996).
[12]S. R. Haskey, B. D. Blackwell, B. Seiwald, M. J. Hole, D. G. Pretty, J. Howard, and J. Wach, Rev. Sci. Instrum. **84**, 093501 (2013).
[13]C. M. Franck, O. Grulke, and T. Klinger, Rev. Sci. Instrum. **73**, 3768 (2002).
[14]B. Sun, G. Y. Yuan, W. G. Huo, and Z. F. Ding, Rev. Sci. Instrum. **81**, 054703 (2010).
[15]Y. X. Liu, Y. S. Liang, D. Q. Wen, Z. H. Bi, and Y. N. Wang, Plasma Sources Sci. Technol. **24**, 025013 (2015).
[16]K. Zhao, Y. X. Liu, E. Kawamura, D. Q. Wen, M. A. Lieberman, and Y. N. Wang, Plasma Sources Sci. Technol. **27**, 055017 (2018).